Eur. Phys. J. B **5**, 53–60 (1998)

THE EUROPEAN PHYSICAL JOURNAL B

Fano-like coupling of collective and particle-hole excitations in Li metal

K. Höppner, A. Kaprolat, and W. Schülke[a]

Institute of Physics, University of Dortmund, 44221 Dortmund, Germany

Received: 29 December 1998 / Accepted: 16 March 1998

Abstract. The dynamic structure factor $S(\mathbf{q},\omega)$ of Li with $\mathbf{q} \parallel [110]$ and 0.88 a.u. $< q <$ 1.03 a.u., as measured with 1 eV resolution by means of synchrotron radiation based inelastic X-ray scattering spectroscopy (IXSS), exhibits, in the energy loss range between 3 and 12 eV, a fine structure, which appears as a resonance around 4 eV and an antiresonance around 8 eV, when the difference between the experimental $S(\mathbf{q}\omega)$-spectra with $\mathbf{q} \parallel [110]$ and $\mathbf{q} \parallel [111]$ is considered. In order to find out the origin of this fine structure we have interpreted recent TLDA (time dependent local density approximation) calculations of the Li-$S(\mathbf{q},\omega)$ [12], which were based on the inversion of the full dielectric matrix, by utilizing a simple two-plasmon-band model. In this way the fine structure can be traced back to a Fano-like coupling of the discrete collective excitations (both the regular plasmon and the so-called zone-boundary collective states (ZBCS's)) and the particle-hole excitation continuum, mediated by the off-diagonal elements of the dielectric matrix, $\varepsilon_{\mathbf{0G}}$, where $\mathbf{G} = (2\pi/a)$ (1,1,0).

PACS. 71.45.Gm Exchange, correlation, dielectric and magnetic functions, plasmons – 78.70.Ck X-ray scattering – 71.20.Dg Alkali and alkaline earth metals

1 Introduction

It is well known [1] that the excitation spectrum of jellium (a free electron system on the background of a continuously distributed positive charge) consists, within the limits of the random phase approximation (RPA), of two contributions, which can be clearly separated: (i) discrete collective excitations (plasmons) for a momentum transfer $q < q_c$ (q_c = plasmon cut-off vector) found in an energy range, which is determined by the plasmon dispersion relation:

$$\hbar\omega_p(q) = \hbar\omega_p(0) + \alpha q^2 \tag{1}$$

where α is the plasmon dispersion coefficient.
(ii) The particle-hole continuum $\hbar\omega(q)$, which extends, for a given momentum transfer q, to the following energy range:

$$\begin{aligned} &0 < \hbar\omega(q) < q^2/2m + qk_F/m \quad \text{for} \quad q < 2k_F \\ &q^2/2m - qk_F/m < \hbar\omega(q) < q^2/2m + qk_F/m \\ &\text{for} \quad q > 2k_F. \end{aligned} \tag{2}$$

Switching on of the periodic lattice potential results in the following modifications of the above simple picture, which are sketched in Figure 1 as calculated for a two-band model described in Section 2 in greater detail:

(i) introducing of umklapp-processes (interband transitions) into the particle-hole excitation continuum makes the collective excitations damped [2].
(ii) The plasmon excitations will form plasmon bands with plasmon energy gaps at the zone boundaries, provided these plasmons are well-defined elementary excitations for q's extending up to the zone boundary. (Plasmon band gaps were not represented in Figure 1, since the plasmon dispersion shown there is the result of a two-band calculation for Li, where the energy position of the two plasmon bands at the zone boundary could not be separated because of the large width of the response function). The existence of these plasmon bands was experimentally verified for the case of Si [3,4], where $q_c > (1/2)G_{111}$ ($\mathbf{G}_{hkl}$ = reciprocal lattice vector).
(iii) The plasmon bands become periodic in the reciprocal lattice, so that the lower plasmon band in the second Brillouin zone of the extended zone-scheme (long-dashed line in Fig. 1) overlaps the particle-hole continuum. It has been shown by Sturm *et al.* [5] and Schülke *et al.* [6] that this overlap can lead to Fano-like (anti)resonances [7] due to the interaction of the discrete plasmon excitations with the continuum of particle-hole excitations.
(iv) Opening of excitation gaps in the particle-hole excitation spectrum can produce additional zeros (or nearly-zeros) of the real part of the dielectric function, $\Re\varepsilon(\mathbf{q},\omega)$, in an energy range of very low values of $\Im\varepsilon(\mathbf{q},\omega)$, so that the condition for additional collective excitations, the so-called zone-boundary collective states (ZBCS's) [8] is

[a] e-mail: schuelke@physik.uni.dortmund.de

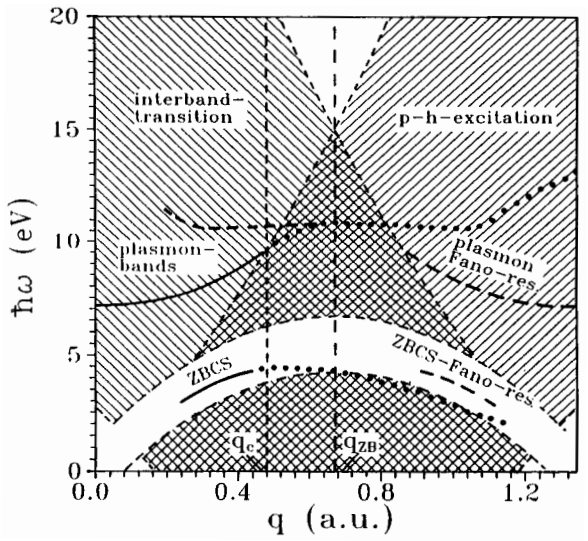

Fig. 1. Illustration of the effect of umklapp processes on the p-h-excitation continuum, both on the regular plasmon excitation branch, and on the ZBCS-branch in the repeated zone scheme of a two-plasmon-band model of Li ($\mathbf{q}||[110]$; $-\mathbf{q}_r = \mathbf{q} - \mathbf{G}$; $\mathbf{G} = (2\pi/a)(1,1,0)$). Solid lines: peak-positions, $\hbar\omega_o$, of $\Im[-\varepsilon^{-1}(\mathbf{q}_r,\omega)_{\mathbf{00}}]$, whenever these peaks represent collective excitations (regular plasmons and ZBCS's, resp.), as characterized by $\Re[\varepsilon_{\mathbf{00}}(\mathbf{q}_r,\omega_o)] = 0$. Long-dashed lines: result of the umklapp process on collective excitations, range of plasmon-Fano-resonances. Short-dashed line: higher plasmon-bands, only schematic. Points: peak-positions of $\Im[-1/\varepsilon_{\mathbf{00}}(\mathbf{q}_r,\omega)]$ and $\Im[-1/\varepsilon_{\mathbf{GG}}(\mathbf{q}_r,\omega)]$, respectively.

satisfied. This type of collective excitations has been verified experimentally for simple metals as Li [9,10] and Be [11].

It should be shown in what follows that:
(i) Fano-like resonances are, besides Si, also detectable in Li metal within a certain range of q-values and distinct directions of $\mathbf{q}$.
(ii) These Fano-like resonances become experimentally verified not only as being due to interference between regular plasmons and the the particle-hole continuum, but also as a consequence of coupling between the ZBCS's and the particle-hole (p-h) continuum, where surprisingly the latter coupling is much stronger than the former one.

The rest of the paper is organized as follows: in Section 2 the optimal $\mathbf{q}$-range for detecting of Fano-like resonances both for regular plasmons and for ZBCS's is defined. Furthermore a two-plasmon-band calculation is presented in order to predict, what type and size of Fano-like resonances can be expected in Li metal. In Section 3 we analyze calculations of the complete dielectric matrix of Li metal, performed within the limits of the time dependent local density approximation (TLDA) by Bross and Ehrnsperger [12], with respect to Fano-like resonances, where the interpretation of our two-plasmon band calculation finds full confirmation. Moreover, these calculations will show the way to what might be the appropriate experimental signature of Fano-like resonances. In Section 4 we present the experimental results on Fano-like resonances in Li metal and compare them with two-plasmon band and TLDA-calculations. Finally in Section 5 conclusions about the underlying models are drawn.

2 Plasmon Fano resonances of Li in a two-plasmon-band model

As pointed out by Sturm *et al.* [5], the dynamic structure factor $S(\mathbf{q},\omega)$ can be written, within the limit of a two-plasmon-band model, in the following form:

$$S(\mathbf{q},\omega) = (\hbar q^2/4\pi^2 e^2 n_o)\Im\{(-1/\varepsilon_{\mathbf{GG}}) + (\varepsilon_{\mathbf{G0}}\varepsilon_{\mathbf{0G}}/\varepsilon^2_{\mathbf{GG}})[-\varepsilon^{-1}(\mathbf{q}_r,\omega)]_{00}\} \times [1/(1 - G^0(|\mathbf{q}_r + \mathbf{G}|))], \quad (3)$$

where $\mathbf{q}_r = \mathbf{q} - \mathbf{G}$ is the momentum transfer, reduced to the first Brillouin zone, and n_o is the mean electron density. $[\varepsilon^{-1}(\mathbf{q}_r,\omega)]_{\mathbf{GG'}}$ is the $\mathbf{GG'}$ element of the inverse of the microscopic dielectric matrix which is defined by

$$\varepsilon_{\mathbf{GG'}}(\mathbf{q}_r,\omega) = \delta_{\mathbf{GG'}} - v_{\mathbf{q}_r+\mathbf{G}}[1-\mathbf{G}^0(|\mathbf{q}_r+\mathbf{G}|)] \times \chi^0(\mathbf{q}_r+\mathbf{G},\mathbf{q}_r+\mathbf{G'},\omega), \quad (4)$$

$v_{\mathbf{q}_r+\mathbf{G}} = 4\pi^2/|\mathbf{q}_r + \mathbf{G}|^2$, $\chi^0(\mathbf{q}_r + \mathbf{G}, \mathbf{q}_r + \mathbf{G'}, \omega)$ is the independent-particle density-density response function, and $G^0(q)$ is a static local-field factor, which corrects approximately for exchange and correlation. It can easily be verified that this way of introducing the local-field factor $G^0(q)$ into the dielectric matrix is equivalent to the usual definition, as given for example by Utsumi and Ichimaru [13] for the case of jellium. (In Eq. (3) the arguments $(\mathbf{q}_r,\omega)$ of $\varepsilon_{\mathbf{GG'}}$ have been suppressed). Equation (3) clearly indicates how a Fano-like plasmon resonance originates: it is the coupling of the discrete long-wavelength collective excitation, represented by $\Im[-\varepsilon^{-1}(\mathbf{q}_r,\omega)]_{\mathbf{00}}$, to the short-wavelength electron-hole-pair excitation continuum, described by $\Im[-1/\varepsilon_{\mathbf{GG}}(\mathbf{q}_r,\omega)]$, which can produce a valley-peak fine structure typical of a Fano resonance, whenever the coupling factor $f_{\mathbf{G}}(\mathbf{q}_r,\omega) = \varepsilon_{\mathbf{G0}}\varepsilon_{\mathbf{0G}}/\varepsilon^2_{\mathbf{GG}}$ has a negative imaginary part, and $\Re[-\varepsilon^{-1}(\mathbf{q}_r,\omega)]$ changes its sign from plus to minus at $\omega = \omega_p(\mathbf{q}_r)$. Additionally, it depends on the sign of the real part of the coupling factor $f_{\mathbf{G}}(\mathbf{q}_r,\omega)$, whether the coupling of the collective excitation, represented by $\Im[-\varepsilon^{-1}(\mathbf{q}_r,\omega)]$ (always positive), will produce a resonance or an antiresonance. In order to find out the most favourable case for detecting plasmon Fano resonances in Li, one has, on the one hand, to realize that the strength of these resonances are determined by the non-diagonal elements $\varepsilon_{\mathbf{0G}}$ of the dielectric matrix, whose value depends mainly on the size of the $\mathbf{G}$-th Fourier component, $V_{\mathbf{G}}$, of the crystal potential. According to Heine and Abarenkov [14], the $\mathbf{G}$-th Fourier components V_{110} and V_{200} of the local pseudopotential of Li are the most prominent ones among all the others. On the other hand, according to Figure 1, $|\mathbf{q}|$ must not be much smaller than $|-\mathbf{q}_c+\mathbf{G}|$, in order that $\Im[-\varepsilon^{-1}(\mathbf{q}_r,\omega)]_{00}$ represents a well

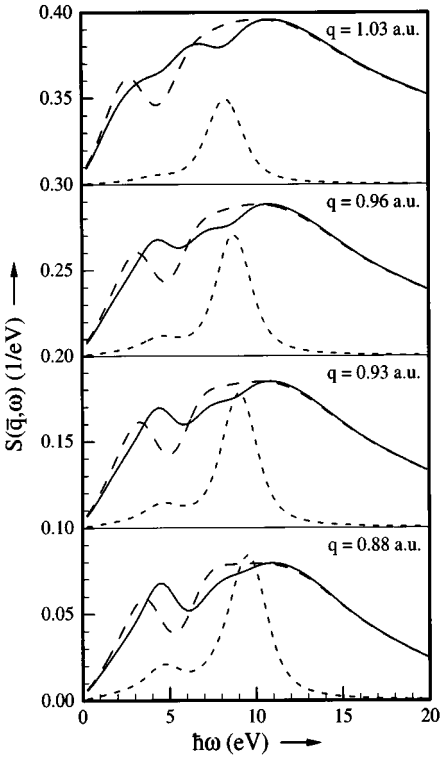

Fig. 2. Response functions of Li for $\mathbf{q}||[110]$; $q = 0.88$ a.u., $q = 0.93$ a.u., $q = 0.96$ a.u. and $q = 1.03$ a.u., respectively, empirical pseudopotential calculation within the limits of a two-plasmon-band model. Solid line: $S(\mathbf{q},\omega)$. Long-dashed line: $S_{\mathbf{G}}(\mathbf{q},\omega)$. Short-dashed line: $S_{\mathbf{0}}(\mathbf{q}_r,\omega)$; $-\mathbf{q}_r = \mathbf{q} - \mathbf{G}$; $\mathbf{G} = (2\pi/a)(1,1,0)$.

defined discrete collective excitation ($q_c = 0.48$ a.u. for Li; a.u. = atomic units: $\hbar = e = m_e = 1$). Moreover, since $\hbar\omega = \mathbf{q}^2/2m$ roughly marks the centre of the electron-hole excitation continuum, and $q^2/2m - k_F q/m$ is its lower boundary, $|\mathbf{q}|$ must not be too far from $[2m\hbar\omega_p(\mathbf{q}_r)]^{1/2}$, and must not be larger than $(2\hbar\omega_p(\mathbf{q}_r) + k_F^2)^{1/2} - k_F$. By taking into account all three constraints on $\mathbf{q}$, the most favourable case is

$$\mathbf{G} = (2\pi/a)(1,1,0), \quad \mathbf{q}||[110],$$
$$|-\mathbf{q}_c + \mathbf{G}_{110}| < |q| < (2\hbar\omega_p(\mathbf{q}_c) + k_F^2)^{1/2} - k_F \qquad (5)$$

(k_F = Fermi momentum). $\mathbf{G}_{200}$ would contribute a strong crystal potential Fourier coefficient, but since $|-\mathbf{q}_c + \mathbf{G}_{200}| \approx [(2\hbar\omega_p(\mathbf{q}_c) + k_F^2)^{1/2} - k_F] \gg [2m\hbar\omega_p(\mathbf{q}_r)]^{1/2}$, the case $\mathbf{q}||[200]$; $\mathbf{G} = (2\pi/a)(2,0,0)$ is not an appropriate candidate for detecting plasmon-Fano-resonances [6]. Cases with other reciprocal lattice vectors than $\mathbf{G}_{110}$ and $\mathbf{G}_{200}$ should not be considered because of the much too small Fourier coefficients of the crystal potential.

We have calculated the plasmon Fano resonances of Li within the limits of the two-plasmon-band model according to equations (3) and (4) with $\mathbf{G} = (2\pi/a)(1,1,0)$; $q||[110]$ and 0.88 a.u. $< |\mathbf{q}| <$ 1.03 a.u. (see Eq. (5)). The dielectric 2×2 matrix was obtained using a two-band (local) pseudopotential scheme with $V_{110} = 0.05$ a.u. [14], a mean effective band mass $m_{eff} = 1.12\, m_e$ [15]. Self-energy (life-time) correction was performed "on-shell", as first proposed in [9], whereby the imaginary part of the self energy, $\Gamma(p) = \Im\sum(p, p^2/2)$, was calculated within the limits of the GW-approximation [16]. The static approximation of the local-field correction factor, $G^0(q)$, of Li was taken over from Utsumi and Ichimaru [13], what seems to be justified for $q < 2k_F$ according to a semi-empirical determination of the local-field correction [17].

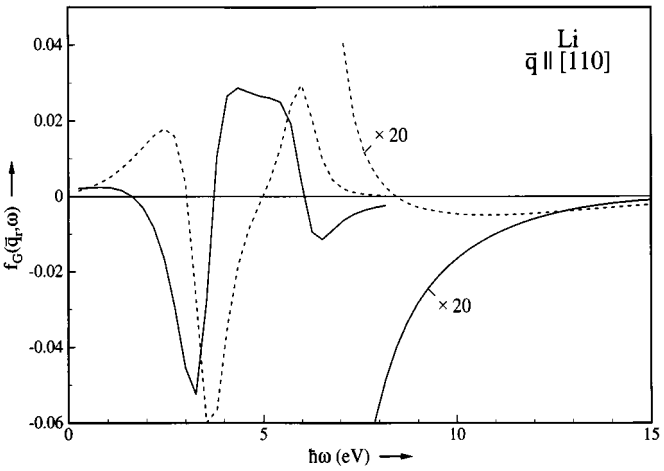

Fig. 3. Coupling factor $f_{\mathbf{G}}(\mathbf{q}_r,\omega)$ of the two-plasmon-band model of Li as a function of $\hbar\omega$. Solid line: $\Re f_{\mathbf{G}}$. Dashed line: $\Im f_{\mathbf{G}}$; $\mathbf{q}$ and $\mathbf{q}_r||[110]$; $\mathbf{G} = (2\pi/a)(1,1,0)$.

In Figure 2 $S(\mathbf{q},\omega)$ according to equations (3) and (4) is plotted for four different values of $|\mathbf{q}|$, together with plots of $S_{\mathbf{0}}(\mathbf{q}_r,\omega) \equiv N(q_r)\Im[-\varepsilon^{-1}(\mathbf{q}_r,\omega)]_{\mathbf{00}}$ ($N(q) = \hbar q^2/4\pi^2 e^2 n_o$), which represents the discrete plasmon excitation, and of $S_{\mathbf{G}}(\mathbf{q},\omega) \equiv N(q)\Im(-1/\varepsilon_{\mathbf{GG}})$, which stands for the electron-hole excitation continuum. All response functions were convoluted with a Gaussian, representing the experimental resolution of 1 eV. One can clearly distinguish two peaks of the plasmon excitation, where the one at higher energy loss is the regular plasmon resonance, whereas the one at lower energy losses must be attributed to what we call a zone-boundary collective state (ZBCS) due to the excitation gap for p-h-excitations into quasi-particle states near the $\mathbf{G}_{110}$-Bragg plane. The dispersion behaviour of these [110]-ZBCS's of Li has already been experimentally verified and thoroughly discussed in [9,10,12]. It should be noticed that remains of this [110]-ZBCS are also detectable in the p-h-continuum. It is clearly visible that the coupling of the conventional plasmon excitation to the p-h-continuum creates an antiresonance with a small valley-peak structure. This behaviour is also confirmed by Figure 3, where the real and imaginary part of the coupling constant $f_{\mathbf{G}}(\mathbf{q}_r,\omega)$ is plotted for the $|\mathbf{q}| = 0.96$ a.u.-case. Both, the real and the imaginary part of $f_{\mathbf{G}}$ are negative within the range of the above mentioned antiresonance, so that the negative real part can be made responsible for the antiresonance and the very small negative imaginary part for the

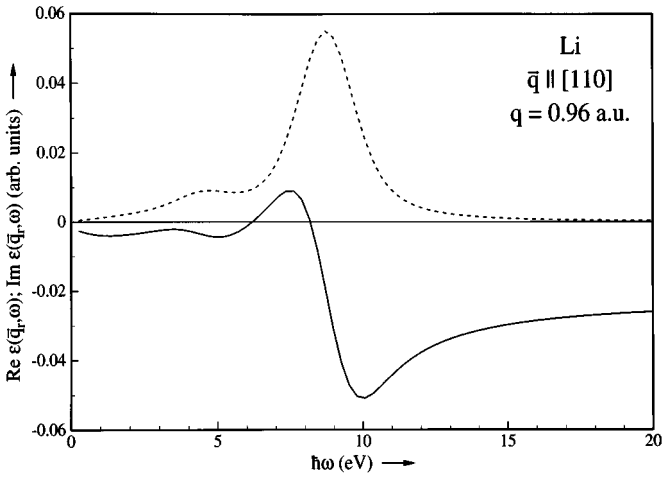

Fig. 4. Solid line: $\Re[-\varepsilon^{-1}(\mathbf{q}_r,\omega)]_{\mathbf{00}}$ of Li. Dashed line: $\Im[-\varepsilon^{-1}(\mathbf{q}_r,\omega)]_{\mathbf{00}}$ of Li, empirical pseudopotential calculation within the limits of a two-plasmon-band model; $-\mathbf{q}_r = \mathbf{q} - \mathbf{G}$; $\mathbf{q}$ and $\mathbf{q}_r$|||[110]; $G = (2\pi/a)(1,1,0)$.

corresponding small valley-peak structure, since the real part of $(-\varepsilon^{-1})_{\mathbf{00}}$ changes its sign from plus to minus near the plasmon resonance (see Fig. 4).

The coupling of the ZBCS to the p-h-continuum produces a very strong Fano-like resonance, characterized by a valley-peak structure, where the peak is much more pronounced than in the former case, typical of a Fano resonance for the case of very strong coupling. Also this behaviour finds confirmation by the plot of $f_{\mathbf{G}}(\mathbf{q}_r,\omega)$: it is the high value of the real part of the coupling constant $f_{\mathbf{G}}(\mathbf{q}_r,\omega)$ and its change of the sign at the ZBCS-peak of $\Im(-\varepsilon^{-1})_{\mathbf{00}}$, which produces the strong valley-peak structure. Moreover, the negative imaginary part of $f_{\mathbf{G}}$ gives rise to an additional resonance in the ZBCS range, since, as indicated in Figure 4, $\Re(-\varepsilon^{-1})_{\mathbf{00}}$ remains negative over the whole range of the ZBCS-resonance.

3 Signatures of plasmon Fano resonances in TLDA calculations

That far we have studied plasmon Fano-resonances only within the limits of a two-plasmon band model, so that the question might arise, to what extent this fine structure of the dynamic structure factor will survive in a first principle calculation, which takes into account the dielectric matrix corresponding to a much greater set of reciprocal lattice vectors. It cannot be excluded that contributions from different reciprocal lattice vectors may destructively interfere. We have used for this purpose TLDA-calculations of Bross and Ehrnsperger [12] who have calculated the dielectric matrix of Li and its inverse for the three principle directions [100], [110] and [111] of $\mathbf{q}$ within a q-range, that covers the relevant range for plasmon Fano resonances [18]. The result of these calculations contains, on the one hand, the response function in the form of the imaginary part of the inverse dielectric matrix, $\Im[-\varepsilon^{-1}(\mathbf{q}_r,\omega)]_{\mathbf{00}}$ and $\Im[-\varepsilon^{-1}(\mathbf{q}_r,\omega)]_{\mathbf{GG}}$, respectively, calculated for a 43×43 dielectric matrix with $\mathbf{q}_r$|||[110] and $\mathbf{G} = (2\pi/a)(1,1,0)$. On the other hand, also the response function in the form of $\Im[-1/\varepsilon_{\mathbf{00}}(\mathbf{q}_r,\omega)]$ and $\Im[-1/\varepsilon_{\mathbf{GG}}(\mathbf{q}_r,\omega)]$ for $\mathbf{q}_r$|||[110] and $\mathbf{G} = (2\pi/a)(1,1,0)$ has been calculated on equal footing, so that plots equivalent to Figure 2 can be presented and compared with the results of the two-plasmon-band calculations. Nevertheless, since the TLDA-data do not exhibit any explicit self-energy correction, they were further processed in the following way, in order to make them better comparable both with the two-plasmon band calculations and to bring them into better agreement with the experimental data. In order to simulate the "on-shell" self-energy correction in an appropriate way, the response functions, for a given $\mathbf{q}_r$, were energy-convoluted with a Lorentzian $L(\omega-\omega')$, whose width was chosen ω-dependent according to the momentum-dependence of the self-energy of the states contributing to the transitions involved, where these states are assumed to be free-electron like:

$$L(\omega-\omega') = [\gamma(\omega)/\pi]/[(\omega-\omega')^2+\gamma^2(\omega)] \tag{6a}$$

$$\gamma(\omega) = [2/(p_u^2-p_l^2)]\int_{p_l}^{p_u} p_\perp[\Gamma(p_i(\omega))+\Gamma(p_f(\omega))]dp_\perp \tag{6b}$$

$$p_0 = \begin{cases} (\hbar\omega/q)-(q/2) & \text{for} \quad |(\hbar\omega/q-(q/2)\le k_F \\ -k_F & \text{for} \quad (\hbar\omega/q)-(q/2) < -k_F \\ k_F & \text{for} \quad (\hbar\omega/q)-(q/2) < k_F \end{cases} \tag{6c}$$

$$p_i^2 = p_0^2 + p_\perp^2 \tag{6d}$$

$$p_f^2 = (p_0+q)^2 + p_\perp^2 \tag{6e}$$

$$p_u^2 = k_F^2 - p_0^2 \tag{6f}$$

$$p_l^2 = \begin{cases} k_F^2-(p_0+q)^2 & \text{for} \quad p_0+q<k_F \\ 0 & \text{else} \end{cases} \tag{6g}$$

$\Gamma(p) = \Im\sum(p,p^2/2)$ was again calculated using the GW-approximation [16]. Additionally the response functions were convoluted with the experimental resolution (Gaussian) of 1 eV. Since the TLDA-calculations were not performed exactly for the q's of the experiment, we have made a linear interpolation of the data between the q-values, which are nearest to the corresponding experimental one.

Figure 5 presents, in analogy to Figure 2, the processed data of the TLDA-calculations, namely $S(\mathbf{q},\omega) \equiv N(q)\Im[-\varepsilon^{-1}(\mathbf{q}_r,\omega)]_{\mathbf{GG}}$ and $S_0(\mathbf{q}_r,\omega) \equiv N(\mathbf{q}_r)\Im[-\varepsilon^{-1}(\mathbf{q}_r,\omega)]_{\mathbf{00}}$, respectively, together with

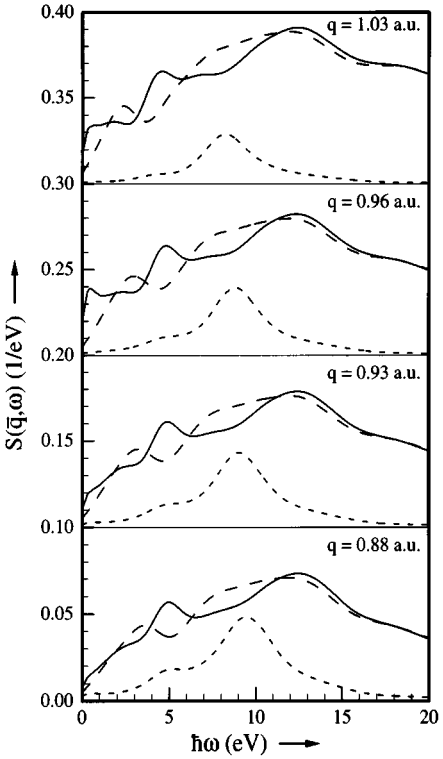

Fig. 5. Response functions of Li for $\mathbf{q}||[110]$; $q = 0.88$ a.u., $q = 0.93$ a.u., $q = 0.96$ a.u. and $q = 1.03$ a.u., respectively, TLDA-calculation. Solid line: $S(\mathbf{q},\omega)$. Long-dashed line: $S_{\mathbf{G}}(\mathbf{q},\omega)$]. Short-dashed line: $S_{\mathbf{0}}(\mathbf{q}_r,\omega)$; $-\mathbf{q}_r = \mathbf{q} - \mathbf{G}$; $\mathbf{G} = (2\pi/a)(1,1,0)$.

$S_{\mathbf{G}}(\mathbf{q},\omega) \equiv N(q)\Im[1/\varepsilon_{\mathbf{GG}}(\mathbf{q}_r,\omega)]$, where $\mathbf{G} = (2\pi/a)(1,1,0)$, for four different values of $\mathbf{q}||[110]$ within the $|\mathbf{q}|$-range marked in equation (5). The resemblance of Figure 5 to Figure 2 is striking, and is explicitely demonstrated by Figure 6, where the corresponding differences between response functions from Figures 2 and 5 are plotted for one value of $|\mathbf{q}|$. It is this resemblance, which makes us to conclude that the most prominent fine structure of $S(\mathbf{q},\omega);\mathbf{q}||[110]$ in the range 3 eV $< \hbar\omega <$ 12 eV must be traced back to the interaction of the $\mathbf{G}_{110}$-induced "umklapp"-plasmons with the p-h-continuum ($\mathbf{q}||[110]$), so that the interpretation of this fine structure as Fano-like resonances stays valid also in the context of the TLDA calculations. The interference with other "umklapp"-processes does not considerably weaken this interaction.

According to Figure 6, the theoretical **calculations** provide signatures of the Fano-like resonances between 3 eV and 12 eV energy loss, both for regular plasmons and for the ZBCS's, in the difference between the [110]-$S(\mathbf{q},\omega)$-spectrum, as obtained by the inversion of the full dielectric matrix, on the one hand, and the [110]-$S(\mathbf{q},\omega)$-spectrum, as calculated from $\Im(-1/\varepsilon_{\mathbf{GG}})$, on the other hand. In order to find signatures of the plasmon-Fano resonances in **experiment**, one has to compare, within the relevant $|\mathbf{q}|$-

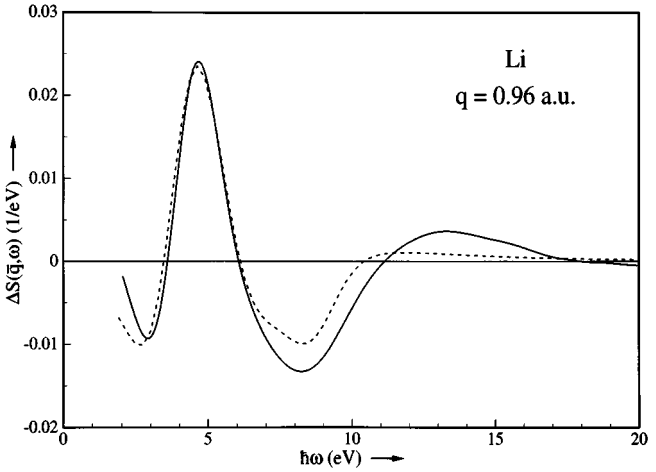

Fig. 6. Solid line: Difference between TLDA-calculated $S(\mathbf{q},\omega)$ and $S_{\mathbf{G}}(\mathbf{q}_r,\omega)$. Dashed line: Difference between pseudopotential-calculated $S(\mathbf{q},\omega)$ and $S_{\mathbf{G}}(\mathbf{q},\omega)$ calculated within the limits of the two-plasmon-band model. Calculations are for Li; $\mathbf{q}||[110]$; $q = 0.96$ a.u.; $\mathbf{G} = (2\pi/a)(1,1,0)$.

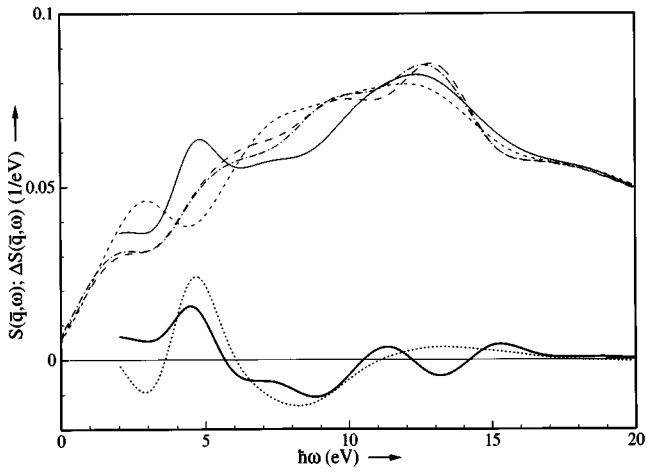

Fig. 7. TLDA-calculated spectra of Li for $q = 0.96$ a.u.: $S(\mathbf{q},\omega)$ for $\mathbf{q}||[110]$ (thin solid line); $S_{\mathbf{G}}(\mathbf{q},\omega)$ for $\mathbf{q}||[110]$ (short-dashed line); $S(\mathbf{q},\omega)$ for $\mathbf{q}||[111]$ (long-dashed line); $S_{\mathbf{G}}(\mathbf{q},\omega)$ for $\mathbf{q}||[111]$ (dashed-dotted line); $\mathbf{G} = (2\pi/a)(1,1,0)$. Thick solid line: Difference between the TLDA-calculated $S(\mathbf{q},\omega)$-spectra with $\mathbf{q}||[110]$ and $\mathbf{q}||[111]$. Dotted line: Difference between TLDA-calculated $S(\mathbf{q},\omega)$- and $S_{\mathbf{G}}(\mathbf{q},\omega)$-spectra with $\mathbf{q}||[110]$.

range, the experimental [110]-$S(\mathbf{q},\omega)$-spectra with spectra for other $\mathbf{q}$-directions, where these spectra should satisfy the following two conditions, (i) they should not exhibit signatures of plasmon Fano resonances in the theoretical calculations, this means, there should not be a marked difference between spectra calculated by the full inversion of the dielectric matrix and those derived from $\Im(-1/\varepsilon_{\mathbf{GG}})$, (ii) these spectra should largely resemble the TLDA-calculated $\mathbf{q}||[110]$-$S_{\mathbf{G}}(\mathbf{q},\omega)$-spectra between 3 and 12 eV, where the signatures for Fano-like resonances are expected.

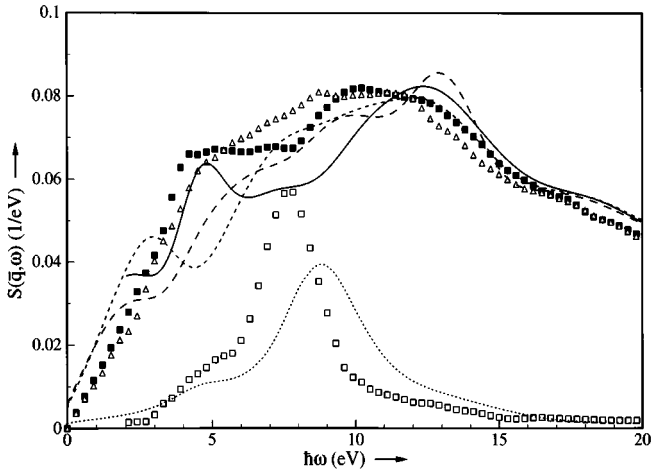

Fig. 8. Solid line: the same as the thin solid line in Figure 7. Short-dashed line: the same as in Figure 7. Long-dashed line: the same as in Figure 7. Dotted line: TLDA-calculated $S_{\mathbf{0}}(\mathbf{q}_r, \omega)$ of Li for $\mathbf{q}_r$||[110], $q_r = 0.38$ a.u. Full squares: experimental $S(\mathbf{q}, \omega)$-spectrum for $\mathbf{q}$||[110]; $q = 0.96$ a.u. Open triangles: experimental $S(\mathbf{q}, \omega)$-spectrum for $\mathbf{q}$||[111]; $q = 0.96$ a.u. Open squares: experimental $S(\mathbf{q}', \omega)$-spectrum for $\mathbf{q}'$||[111]; $|\mathbf{q}'| = |\mathbf{q} - \mathbf{G}_{110}|$; $q' = 0.38$ a.u.; $q = 0.96$ a.u.

It is shown in Figure 7 that the $\mathbf{q}$||[111]-spectra satisfy these conditions quite well, so that they can serve as appropriate reference spectra for demonstrating the existence of plasmon-Fano resonances in the experiment.

4 Measurements of plasmon Fano resonances in Li metal; discussion of the results

We have measured the double differential scattering cross section of single crystal Li metal with $\mathbf{q}$||[110] and $\mathbf{q}$||[111] for $q = 0.38$; 0.88; 0.93; 0.96 and 1.03 a.u. with 1 eV resolution using synchrotron radiation from the DORIS storage ring at DESY, Hamburg, monochromatized to 7.99 keV by means of a Ge(311) double crystal monochromator, and by employing a Si(444) spherically bent analyzer. The experimental setup used is described in detail elsewhere [19]. Contrary to former $S(\mathbf{q}, \omega)$-measurements on Li (see Ref. [9]) we have performed the measurements now on a much finer q-grid within a q-range, which has been carefully selected in order to meet the conditions for plasmon-Fano-resonances as formulated in Sections 2 and 3. The data processing for getting $S(\mathbf{q}, \omega)$ from the measured scattering cross sections is presented in [9]. It should explicitely be mentioned that all experimental data between 0 and 2 eV are less reliable because of the overlap with the rather strong quasi-elastically scattered line.

One example of these measurements, both the [110]-$S(\mathbf{q}, \omega)$- and the [111]-$S(\mathbf{q}, \omega)$-spectrum for $q = 0.96$ a.u. as well as the [110]-$S(\mathbf{q}', \omega)$-spectrum for $q' = |\mathbf{q} - \mathbf{G}_{110}| = 0.38$ a.u. is plotted in Figure 8 together with the results of corresponding calculations, as already shown separately in Figure 7, namely both the TLDA-[110]-$S(\mathbf{q}, \omega)$- and the [111]-$S(\mathbf{q}, \omega)$-spectrum for $q = 0.96$ a.u. as obtained by the inversion of the dielectric matrix, and the TLDA-$S_{\mathbf{G}}(\mathbf{q}, \omega)$-spectrum. Moreover, also the TLDA-[110]-$S(\mathbf{q}_r, \omega)$-spectrum for $q_r = 0.38$ a.u. is shown. One can easily recognize the relevant signatures of the plasmon-Fano-resonances in the experimental data, both with respect to the conventional plasmons and to the ZBCS's: (i) the deep dip (antiresonance) in the continuum of the [110]-spectrum, when compared with the continuum of the [111]-spectrum, at $\hbar\omega = 7.6$ eV, just at the experimental position of the conventional plasmon for $\mathbf{q}_r = \mathbf{q} - \mathbf{G}_{110}$. It should be noted that the dip-position is likewise shifted to lower energy losses by roughly 1 eV, when compared with the calculations, as the position of the regular plasmon does; (ii) the shoulder (resonance) in the continuum of the [110]-spectrum, when compared with the continuum of the [111]-spectrum, at 4.0 eV, just at the experimental position of the shoulder of the [110]-spectrum for $q_r = 0.38$, which must be attributed to a ZBCS. In order to demonstrate these very clear signatures for plasmon-Fano resonances, which are common in all experimental results, we have plotted in Figures 9a to 9d the corresponding differences, namely the experimental differences between the [110]- and the [111]-spectra for $q = 0.88$; 0.93; 0.96 and 1.03 a.u., respectively, the difference between the TLDA-calculated [110]- and [111]-spectrum from the matrix inversion, and the difference between the TLDA-[110]-$S(\mathbf{q}, \omega)$ spectrum from the matrix inversion and the TLDA-[110]-$S_{\mathbf{G}}(\mathbf{q}, \omega)$-spectrum. Moreover, the same difference as calculated within the limits of the plasmon-two-band model is shown. We find for all q-values the valley in the experimental difference spectrum around 8 eV to be a strong signature of the plasmon-Fano antiresonance as predicted by the TLDA- and the two-plasmon-band-calculations. The valley position is shifted by roughly 1 eV to lower energy losses, when compared with the calculation, in agreement with the corresponding shift to lower energy losses of the experimental regular plasmon peak. Likewise the peak in the experimental difference spectrum around 4 eV is found for all q-values to be a signature of the ZBCS-Fano-resonance as predicted both by the TLDA- and the two-plasmon-band-calculations, where the experiment agrees much better with the TLDA-calculated [110]-[111] differences than with the other ones. This must be expected according to the calculations presented in Figure 7: the resemblance between the TLDA-[111]-$S(\mathbf{q}, \omega)$- and the $S_{\mathbf{G}}(\mathbf{q}, \omega)$-spectra is not so good in that ω-region. It should still be noted that the supplementary ("on-shell")-self-energy correction of the TLDA-calculations have lead to a rather good agreement of the spectra with experiment, certainly with one exception: the overall spectral weight of the calculations as compared with the experiment is less for 4 eV$< \hbar\omega <$ 12 eV and somewhat larger for 12 eV$< \hbar\omega <$ 20 eV. This discrepancy might be attributed to the fact that the local-field correction implicitely performed within the TLDA-scheme is not properly done, as already stated by Fleszar *et al.* [20] for the case of Al.

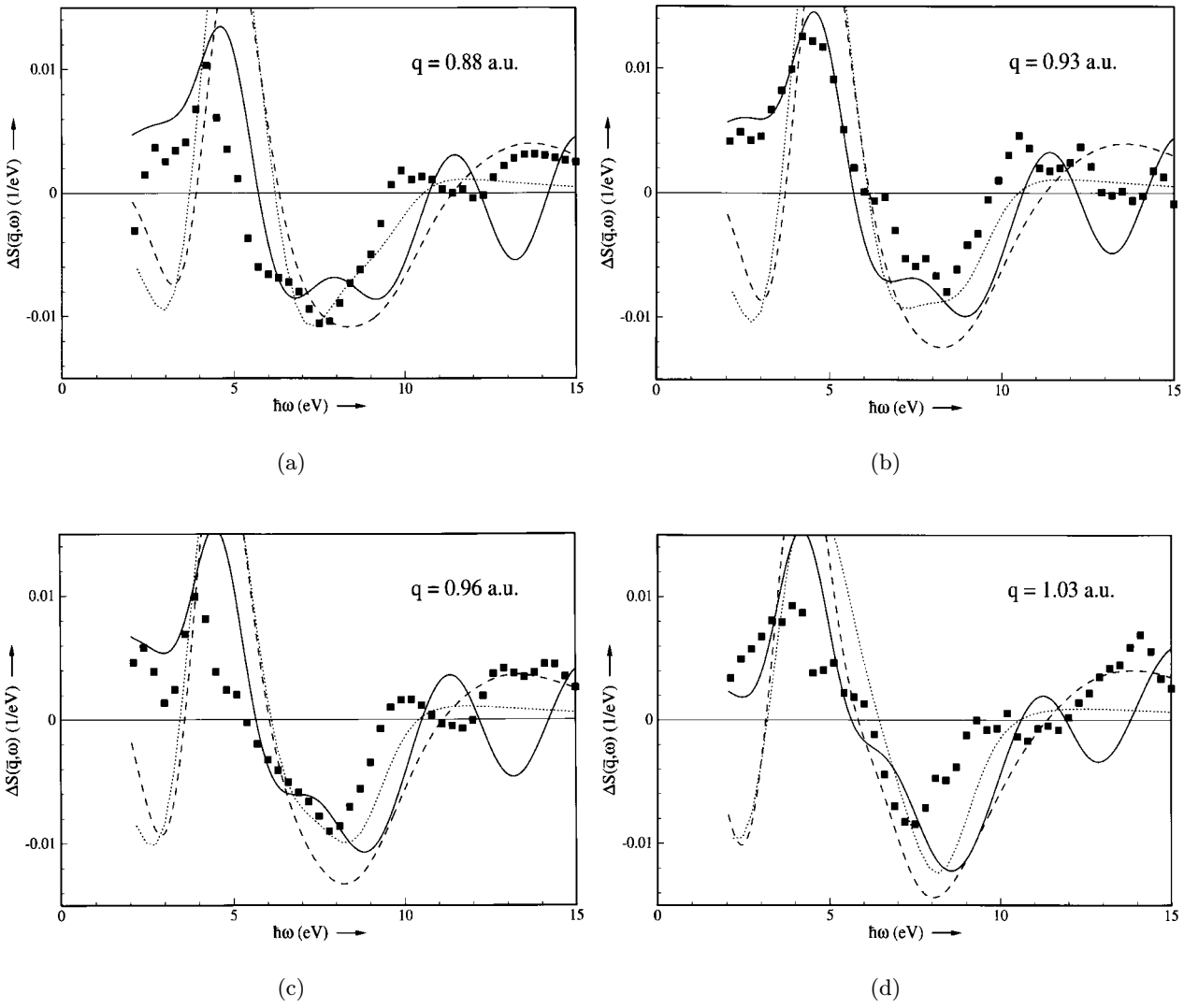

Fig. 9. Solid line: difference between TLDA-calculated $S(\mathbf{q},\omega)$-spectra of Li with $\mathbf{q}||[110]$ and $\mathbf{q}||[111]$. Dashed line: difference between TLDA-calculated $S(\mathbf{q},\omega)$ and $S_{\mathbf{G}}(\mathbf{q},\omega)$ of Li with $\mathbf{q}||[110]$. Dotted line: difference between the two-plasmon-band calculated [110]-$S(\mathbf{q},\omega)$- and the two-plasmon-band calculated [110]-$S_{\mathbf{G}}(\mathbf{q},\omega)$-spectrum of Li. Full squares: difference between the experimental $S(\mathbf{q},\omega)$-spectra of Li with $\mathbf{q}||[110]$ and $\mathbf{q}||[111]$. (a) $q = 0.88$ a.u., (b) $q = 0.93$ a.u., (c) $q = 0.96$ a.u. and (d) $q = 1.03$ a.u., respectively, $\mathbf{G} = (2\pi/a)(1,1,0)$.

5 Conclusions

In conclusion, we have found strong indications of Fano-like coupling of collective and particle-hole excitations in the measured dynamic structure factor $S(\mathbf{q},\omega)$ of Li metal for $\mathbf{q}||[110]$, where the collective excitations could either be the regular plasmons or zone-boundary collective states (ZBCS's). The signatures for the corresponding Fano-(anti)resonances were found by interpreting calculations of the microscopic dielectric matrix, performed within the limits of the time-dependent local density approximation (TLDA), in terms of a two-plasmon-band model. This way the productivity of the plasmon-Fano resonance concept for analyzing of experimental response functions with respect to crystalline local fields could be established.

We thank H. Bross and M. Ehrnsperger of the ML University of Munich for providing the full set of their TLDA-caculations of the full dielectric matrix of Li metal. We thank R. Heise and K.-J. Gabriel for valuable help with the measurements. This work was funded by the German Federal Ministry of Education, Science, Research and Technology under contract No. 05 650WEA.

References

1. D. Pines, P. Nozières, *The Theory of Quantum Liquids* Vol. 1. (Banjamin, New York 1966).
2. W.M. Saslow, G.F. Reiter, Phys. Rev. B **7**, 2995 (1973).
3. W. Schülke, A. Kaprolat, Phys. Rev. Lett. **67**, 879 (1991).
4. K. Sturm, W. Schülke, Phys. Rev. B **46**, 7193 (1992).
5. K. Sturm, W. Schülke, J.R. Schmitz, Phys. Rev. Lett. **68**, 228 (1992).
6. W. Schülke, J.R. Schmitz, H. Schulte-Schrepping, A. Kaprolat, Phys. Rev. B **52**, 11 721 (1995).
7. U. Fano, Phys. Rev. **124**, 1866 (1961).
8. E.-Ni Foo, J.J. Hopfield, Phys. Rev. **173**, 635 (1968).
9. W. Schülke, H. Nagasawa, S. Mourikis, P. Lanzki, Phys. Rev. B **33**, 6744 (1986).
10. E. Burkel, Z. Naturforsch. **48a**, 289 (1993).
11. W. Schülke, H. Nagasawa, S. Mourikis, A. Kaprolat, Phys. Rev. B **40**, 12 215 (1989).
12. H. Bross, M. Ehrnsperger, Z. Phys. B **97**, 17 (1995).
13. K. Utsumi, S. Ichimaru, Phys. Rev. A **26**, 603 (1982).
14. V. Heine, I. Abarenkov, Philos. Mag. **9**, 451 (1964).
15. R.W. Shaw, J. Phys. C (Solid St. Phys.) **2**, 2350 (1969).
16. L. Hedin, S. Lundquist, in *Solid State Physics* 23, edited by Ehrenreich, F Seitz, D. Turnbull (Academic, New York, 1969) p. 1.
17. W. Schülke, K. Höppner, A. Kaprolat, Phys. Rev. B **54**, 464 (1996).
18. The authors greatly appreciate that H. Bross and M. Ehrnsperger have provided the full set of numerical data of their calculations in a form, which could be easily further processed.
19. A. Berthold, S. Mourikis, J.R. Schmitz, W. Schülke, H. Schulte-Schrepping, Nucl. Instrum Methods Phys. Res. A **317**, 373 (1992).
20. A. Fleszar, A.A. Quong, A.G. Eguiluz, Phys. Rev. Lett **74**, 590 (1995).